Gazi University Journal of Science
GU J Sci
24(4):883-899(2011)

Parametric Study of A Single Cell Proton Exchange Membrane Fuel Cell For A Bundle of Straight Gas Channels

Atilla BIYIKOĞLU[♠,1, 2], Ceren Özge ALPAT[3]

[1] *Gazi University, Faculty of Engineering, Mechanical Engineering Department, Celal Bayar Boulevard, 06570 Maltepe, Ankara TURKEY*

[2]*Clean Energy Research and Application Center (CERAC), Gazi University*
[3]*Ostim OSB, Ankara, KLISOM A.Ş TURKEY*

Received: 16.02.2011 Accepted: 26.03.2011

ABSTRACT

In this analysis, a single cell proton exchange membrane (PEM) fuel cell model was constructed in a three dimensional coordinate system. The effects of operating pressure and mass flow rate of the cathode and anode gases on the fuel cell characteristics were investigated parametrically. Besides, the mass fraction of water at the cathode side and the mass fraction of hydrogen at the anode side were selected as investigation parameters and their effects were presented on the polarization curves. The model was tested at the atmospheric pressure based on an experimental result existing in the literature. It was observed that the current density had not been sensitive to any changes in the mass flow rate of the anode gases unlike the cathode gases'. It was also observed that there were current limitations which were more dominant over the water rather than the hydrogen.

Key Words*: PEM fuel cell, straight gas channels, polarization curve, parametric study.*

♠Corresponding author, e-mail: abiyik@gazi.edu.tr

1. INTRODUCTION

The solution of models developed for the transport phenomena in the fuel cells requires much computational time due to complex mechanisms that govern the transport field. However, presenting the results as polarization curves tremendously increases the time spent for the study. In this respect, it may be more suitable to use the commercial computational fluid dynamics (CFD) codes rather than the one developed by the user. A few examples are presented in the references through [1] to [8]. Some of the researchers prefer to present the results as polarization curves which make the study more meaningful. Example studies are selected from the literature and described below;

Um et al. [9] were predicted the polarization curves of under the hydrogen dilution conditions which had been in qualitative agreement with the recent experiments reported in the literature. Wang et. al. [10] were studied the PEM fuel cell experimentally and numerically, and presented the results in the form of polarization curves, which show the effects of the various operating parameters on the performance of the PEM fuel cell.

The following selected studies are some of the examples of FLUENT package usage in the PEMFC technology: A unified, 3D, steady-state numerical mass-transfer single cell model for the PEMFC were solved by Kumar and Reddy [11] using FLUENT 6.0 with GAMBIT 2.0 as a pre-processor. The average current density values were calculated at a different permeability of the metal foam in the flow-field for the multi-parallel flow-field channel design.

Jiao, Zhou and Quan [12] were presented a numerical investigation of the air–water flow in parallel serpentine channels on the cathode side of a PEM fuel cell stack by the use of FLUENT. The different air–water flow behaviors inside the serpentine flow channels with the inlet and outlet manifolds were discussed. The several gas flow problems of parallel serpentine channels were identified and the flow patterns inside the channels and manifolds were investigated.

Quan and Lai [13] were numerically investigated the water management in the air flow channel of a PEMFC cathode using the FLUENT software package. The effects of the channel surface hydrophilicity, channel geometry, and air inlet velocity on the water behavior, water content inside the channel, and two-phase pressure drop were discussed in detail.

In their studies of Jiao and Zhou [14], the three innovative gas diffusion layers (GDL) with different micro-flow channels were proposed and the air–water flow across the GDLs together with a serpentine gas flow channel on the PEM fuel cell cathode was solved by the use of FLUENT.

In this study, a single cell having the nine straight channels on the both side of polar collectors was taken into account. The conventional bundles of parallel channels were selected as an initial study to see the effect of channel configuration and settlement throughout the polar plate for the future investigations. Polarization curves were constructed for different operating conditions.

2. DESCRIPTION OF THE MODEL

The model was comprised of a single cell and the bundle of gas channels on the both current collectors. The gas channels were equally distributed to both the cathode and anode sides of the cell, nine of them on the cathode current collector. The bundle was included totally eighteen gas channels and the components of the model are explicitly shown in Figure 1.

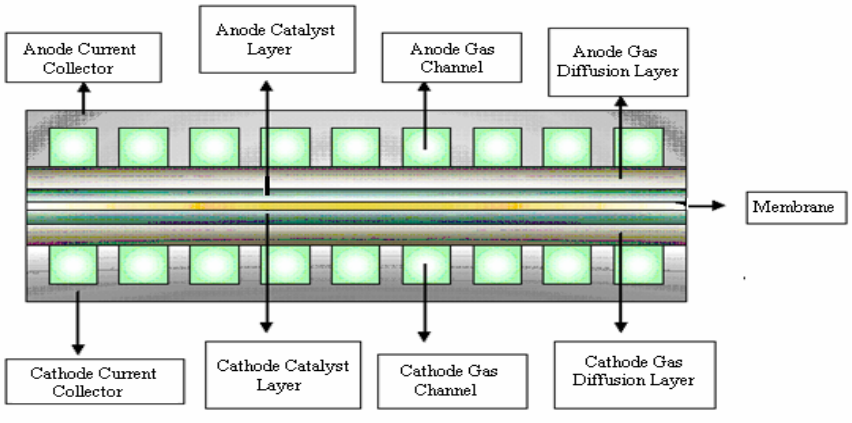

Figure 1. Schematic view of the PEM fuel cell.

Table 1.Physical parameters of PEM Fuel Cell [1].

Parts	Width / mm	Height / mm	Length / mm
Current collector	19	2	70
Gas channels	1	1	70
Gas diffusion layer	19	0.3	70
Catalyst layer	19	0.0129	70
Membrane	19	0.108	70
PEMFC	19	4.7338	70

The membrane electrode assembly (MEA) of the fuel cell was an active area of 13.3 cm^2. The physical and electrochemical parameters of the cell are presented in Table 1 and 2, respectively. The total height of the PEM fuel cell for one cell was 4,734 mm. The catalyst material was selected as platinum to increase the rate of electrochemical reactions due to low working temperature of the PEM fuel cell and the current collector material as graphite due to high electrical conductivity. Toray (8TGP-H-060) paper was used for the GDL and nafion for the membrane. The property values are summarized in Table 3 for each component of the PEM fuel cell.

Table 2.Electrochemical parameters [1-3].

Electrochemical Parameters	**Values**
Anode reference current density [2]	$1.0x10^9$ A m^{-3}
Anode reference molar concentration [1]	0.546 kmol m^{-3}
Anode concentration exponent [3]	0.25
Anode exchange coefficient [3]	1.5
Cathode reference current density [2]	20000 A m^{-3}
Cathode reference molar concentration [1]	0.00339 kmol m^{-3}
Cathode concentration exponent [3]	0.5
Cathode exchange coefficient [3]	2
Open circuit voltage	1.18 V
Hydrogen reference diffusivity [2]	$7.33x10^{-5}$ m^2 s^{-1}
Oxygen reference diffusivity [2]	$2.13x10^{-5}$ m^2 s^{-1}
Water reference diffusivity [2]	$7.33\ x10^{-5}$ m^2 s^{-1}
Species reference diffusivity [2]	$4.90\ x10^{-5}$ m^2 s^{-1}

The transport phenomena inside the PEM fuel cell were modeled for a single cell in a three-dimensional Cartesian coordinate system. The governing equations of continuity, momentum, energy, and species concentrations of different components of a fuel cell, as well as the equations for phase potential in the membrane and catalyst layer were coupled with chemical reaction kinetics by introducing the source terms. The model assumptions can be listed as follows[15]; Ideal gas mixtures; Incompressible and laminar flow due to small pressure gradients and Reynolds numbers; The effective diffusion coefficient of the reactant gases in the porous media was constant; the gas flow through the diffuser and catalyst layers was transported via only diffusion; The diffusion layer, catalyst layer and membrane were isotropic and homogeneous, characterized by effective permeability and uniform porosity; the catalyst layers were assumed to be very tin and allow only current flow; the Butler–Volmer kinetics was governed the electrochemical reaction; The water produced by an electrochemical reaction at the cathode side was in the vapor state; The membrane and catalyst layers were taken as a single layer; The membrane had homogeneous structure and fully saturated with water; The membrane was impervious for the reactant gases; the ohmic losses were ignored inside the diffusion layers and current collectors.

Table 3. Physical properties of PEMFC components [3-6].

Physical Properties	**CC**	**GDL**	**CL**	**M**
Density / kg m^{-1}	2100 [4]	450 [4]	1240 [4]	2000 [4]
Specific heat / J kg^{-1} m^{-1}	1100 [4]	730 [4]	0,225 [4]	500 [4]
Thermal conductivity / W m^{-1} K^{-1}	20 [4]	20 [4]	0,24 [4]	70 [4]
Electrical conductivity / Ohm^{-1} m^{-1}	10^4 [4]	1250 [4]	1250 [4]	-
Porosity	-	0,4 [4]	0,28 [5]	-
Viscous resistance / m^{-2}	-	$1.2x10^{-12}$ [6]	$1.2x10^{-12}$ [6]	-
Permeability / m^2	-	$1.76x10^{-11}$	-	$1.8x10^{-18}$
Equivalent weight / kg mol^{-1}	-	-	-	1.1 [4]
Proton transfer coefficient	-	-	-	3 [3]

The fuel cell operation was governed by the mass, momentum, species and charge conservation equations. The conservation equations of the mass, momentum, species and charge that were suited for FLUENT 6.2 using a single domain formulation, are as follows:

The continuity equation is given in the following form,

$$\frac{\partial(\rho\varepsilon)}{\partial t}+\nabla\cdot(\varepsilon\rho\vec{u})=S_m \quad (1)$$

where ε is the porosity of the porous media, which is equal to unit for the gas channels, ρ the density, and $\vec{u}$ the intrinsic fluid velocity vector, $\varepsilon\vec{u}$ reflects the superficial velocity in the porous media. The symbol S_m denotes source term for mass production.

The conservation of momentum can be expressed as,

$$\frac{\partial(\rho\varepsilon\vec{u})}{\partial t}+\nabla\cdot(\rho\varepsilon\vec{u}\vec{u})=-\varepsilon\nabla p+\nabla\cdot(\varepsilon\mu\nabla\vec{u})+\vec{S}_u \quad (2)$$

where p represents the static pressure, and $\vec{S}_u$ for the external force.

The conservation of species takes the following form,

$$\frac{\partial(\varepsilon C_k)}{\partial t}+\nabla\cdot(\varepsilon\vec{u}C_k)=\nabla\cdot(D_k^{eff}\nabla C_k)+S_k \quad (3)$$

The diffusivities in the species concentration equations were modified using the Bruggman correlation to account for the porous electrodes, which can be expressed as:

$$D_k^{eff}=\varepsilon_m^{1.5}D_k \quad (3a)$$

In Eq. (3), S_k stands for the volumetric source term for the species equations (kg m^{-3} s^{-1}) due to the electro-chemical reactions and is given by

$$S_k=-\frac{M_{w,k}}{nF}R_j,$$
$$k=H_2,O_2,H_2O;\ \mathrm{n}=2,4;\ \mathrm{j}=\mathrm{an},\ \mathrm{or}\ \mathrm{cat} \quad (3b)$$

For the anode reaction, when the hydrogen is consumed, n value is taken as 2. For the cathode reaction, when the oxygen is consumed, n is taken as 4, and when the water is produced, n is taken as 2.

The conservation of energy can be presented in terms of enthalpy as,

$$\frac{\partial(\rho\varepsilon h)}{\partial t}+\nabla(\rho\varepsilon\vec{u}h)=\nabla(k^{eff}\nabla T)+S_h \quad (4)$$

where S_h holds for the volumetric source terms for the energy equation (W m^{-3}) due to the ohmic heating, heat of formation of water, electric work and latent heat of water, and is given by

$$S_h=h_{react}-R_{an,cat}\eta_{an,cat}+I^2R_{ohm}+h_L \quad (5)$$

where h_{react} is the net enthalpy change due to the electrochemical reactions, the term $R_{an,cat}\eta_{an,cat}$ is the product of the transfer current and the over potential in the anode or the cathode catalyst layer, R_{ohm} is the ohmic resistivity of the conducting media, and h_L is the enthalpy change due to the condensation/vaporization of water.

The conservation of charge is given by the following equation,

$$\nabla\cdot(\sigma_e^{eff}\nabla\Phi_e)+S_\Phi=0 \quad (6)$$

where Φ_e denotes the electrolyte (membrane) or solid phase potential. The source term in Eq. (6) are also called the exchange current density (A m^{-3}) and given by for the membrane phase,

$$S_\Phi=R_{mem}=\begin{cases}+R_{an}\\-R_{cat}\end{cases} \quad (6a)$$

and the solid phase,

$$S_\Phi=R_{sol}=\begin{cases}-R_{an}\\+R_{cat}\end{cases} \quad (6b)$$

and the ionic conductivity for the membrane phase potential was modified using the Bruggman correlation to

account for the porous electrodes, which can be expressed as:

$$\sigma_e^{eff} = \varepsilon_m^{1.5}\sigma_e \tag{6c}$$

The local current density is calculated as,

$$I(x,z) = \sigma_e^{eff}\frac{\partial \Phi_e}{\partial x} \tag{7}$$

and the average current density [8] as

$$I_{avg} = \frac{1}{A}\iint_A I(x,z)dxdz \tag{8}$$

The conservation of mass, momentum and energy were solved in the gas channels and diffusion layers. The conservation of momentum for the porous media was reduced to the Darcy's Law. The heterogenic reactions were assumed to occur at the surface of catalyst layers.

In the PEM fuel cell model, the solution was obtained by assuming the chemical reactions to be heterogeneous and to occur on the side of the catalyst facing to the membrane. The potential difference between the catalyst layers and membrane was driving force for the reaction to occur and was called as activation loss or surface over-potential. The potential difference between the anode and cathode current collectors was called as external-circuit voltage. The current transfer on the catalyst layers was calculated using the Butler-Volmer equality.

In the PEM fuel cell model of FLUENT, the two electric potential fields were solved. One of the potential fields was solved in the membrane and catalyst layers, and the other was solved in the catalyst layers, diffusion layers, and current collectors. The surface reactions on the porous catalyst region were solved and the reaction diffusion balance was applied to compute the rates. Based on the cell voltage prescribed, the current density value was computed.

3.THE GENERALIZED CONSERVATION EQUATION

The steady state conservation equations including the continuity, momentum, energy, species and charge can be written in the same structure like that

$$\frac{\partial}{\partial x_i}(\rho u_i \phi) = \frac{\partial}{\partial x_i}\left(\Gamma_\phi \frac{\partial \phi}{\partial x_i}\right) + S_\phi \tag{9}$$

where the symbol ϕ represents a dependent variable, Γ_ϕ which stands for the effective diffusion coefficient and S_ϕ represents the source term per unit volume for the variable ϕ. Table 4 gives the different forms of Γ_ϕ and S_ϕ terms corresponding to the related conservation equations.

Table 4.Terms in the Generalized Conservation Equation

Conservation Equation	ϕ	Γ_ϕ	S_ϕ
Continuity	1	0	0
Momentum	u_i	μ_{eff}	S_u
Energy	h	μ_{eff}/σ_h	S_h
Species	m_k	μ_{eff}/σ_k	S_k
Charge	Φ	σ_e^{eff}	S_Φ

The source terms were taken different forms at each PEMFC layer and these are summarized in Table 5. The detailed forms of source terms for the species and potential at the anode and cathode catalyst layers are given in Table 6.

Table 5.Conservation equations and source terms.

Conservation Equations		Source Terms				
		Current Collector	Gas Channels	Gas Diffusion Layer	Catalyst Layer	Membrane
Mass	$\nabla\cdot(\varepsilon\rho\vec{u})=S_m$	$S_m=0$	$S_m=0$	$S_m=0$	$S_m=\sum_k S_k$	$S_m=0$
Momentum	$\nabla\cdot(\rho\varepsilon\vec{u}\vec{u})=-\varepsilon\nabla p+\nabla\cdot(\varepsilon\mu\nabla\vec{u})+\vec{S}_u$	$S_u=0$	$S_u=0$	$S_u=-\frac{\mu}{K}\varepsilon^2\vec{u}$	$S_u=0$	$S_u=0$
Species	$\nabla\cdot(\varepsilon\vec{u}C_k)=\nabla\cdot(D_k^{eff}\nabla C_k)+S_k$	$S_k=0$	$S_k=0$	$S_k=0$	$S_k=-\frac{M_{w,k}}{nF}R_{an}$, $k=H_2$; n = 2 $S_k=-\frac{M_{w,k}}{nF}R_{cnt}$, $k=O_2$; n = 4 $k=H_2O$; n = 2	$S_k=0$
Solid Phase Potential	$\nabla.(\sigma_{sol}\nabla\phi_{sol})+S_{\phi,sol}=0$	$S_{\phi,sol}=0$	$S_{\phi,sol}=0$	$S_{\phi,sol}=0$	$S_{\phi,sol}=-R_{an}$ $S_{\phi,sol}=R_{cat}$	$S_{\phi,sol}=0$
Membrane Potential	$\nabla.(\sigma_{mem}\nabla\phi_{mem})+S_{\phi,mem}=0$	$S_{\phi,mem}=0$	$S_{\phi,mem}=0$	$S_{\phi,mem}=0$	$S_{\phi,mem}=R_{an}$ $S_{\phi,mem}=-R_{cat}$	$S_{\phi,mem}=0$
Energy	$\nabla(\rho\varepsilon\vec{u}h)=\nabla(k^{eff}\nabla T)+S_h$	$S_h=I^2R_{ohm}$	$S_h=0$	$S_h=I^2R_{ohm}$	$S_h=h_{reaction}-R_{an,cat}\eta_{an,cat}+I^2R_{ohm}+h_L$	$S_h=0$

Table 6. Forms of source terms and current density for catalyst layers

Terms	Anode Catalyst Layer	Cathode Catalyst Layer
Species Source Term S_k	$S_{H_2} = -\frac{M_{w,H_2}}{2F} R_{an}$; $S_{H_2O} = 0$	$S_{O_2} = -\frac{M_{w,O_2}}{4F} R_{cat}$; $S_{H_2O} = \frac{M_{w,H_2O}}{2F} R_{cat}$
Current Density $R\left(Am^{-3}\right)$	$R_{an} = j_{an}^{ref}\left(\frac{[H_2]}{[H_2]_{ref}}\right)^{\gamma_{an}}\left(e^{\alpha_{an}F\eta_{an}/RT}\right)$	$R_{cat} = j_{cat}^{ref}\left(\frac{[O_2]}{[O_2]_{ref}}\right)^{\gamma_{cat}}\left(e^{-\alpha_{cat}F\eta_{cat}/RT}\right)$

3.1. The Boundary Conditions

In this study, the "mass flow inlet" and "pressure outlet" boundary conditions were assigned at the inlet and outlet ports of the anode and cathode gas channels, respectively. The "wall" boundary condition was assigned at the surfaces of current collector that faces with the gas channels and outside air. The "porous jump" boundary condition was assigned at the interface between the membrane and catalyst layers, and between the gas diffusion layers and gas channels. The details of boundary conditions that were assigned to the surfaces of each layer of the PEM fuel cell were summarized in Table 7 and 8.

4. NUMERICAL METHOD

In this study, the conservation equations were discretized based on the first order upwind scheme. The relaxation parameter for the velocities and pressure was determined as 0.3 to get the converged solution. The SIMPLE was used as the solution algorithm for the discretized quantities.

The hexagonal grid structure was to be selected for meshing due to the small aspect ratio, 0.4×10^{-2} and insufficient capacity of computer memory. The tests for the grid independent solutions were performed to obtain the optimum number of grid points. For this purpose, the five different distributions of the element numbers were determined varying the interval size of grid structure as shown in Table 9. The distribution of number of elements for each layer is also reported in Table 9.

Table 7.Conservation equations and boundary conditions of anode side of PEMFC.

	Conservation equations	Boundary conditions of anode side through x, y and z axes				
		ACC	AGC	AGDL	ACL	Membrane
Mass	$\nabla(\rho\varepsilon\vec{u}) = S_m$	ZDF - ZDF	ZDF - ZDF	ZDF - ZDF	ZDF - ZDF	ZDF - ZDF
		ZDF - ZDF	PJ - ZDF	PJ - ND	ND - PJ	PJ - PJ
		ZDF - ZDF	MFI - SV=0	ZDF - ZDF	ZDF - ZDF	ZDF - ZDF
Momentum	$\nabla(\rho\varepsilon\vec{u}\vec{u}) = -\varepsilon\nabla p + \nabla\cdot\varepsilon\mu\nabla\vec{u} + S_u$	NS - NS	NS - NS	NS - NS	NS - NS	NS - NS
		NS - NS	PJ - NS	PJ - ND	ND - PJ	PJ - PJ
		NS - NS	MFI - PO (P=0)	NS - NS	NS - NS	NS - NS
Species	$\nabla(\varepsilon\vec{u}C_k) = \nabla(D_k^{eff}\nabla C_k) + S_k$	ZDF - ZDF	ZDF - ZDF	ZDF - ZDF	ZDF - ZDF	ZDF - ZDF
		ZDF - ZDF	PJ - ZDF	PJ - ND	ND - PJ	PJ - PJ
		ZDF - ZDF	MFI - SV=0	ZDF - ZDF	ZDF - ZDF	ZDF - ZDF
Solid phase potential	$\nabla.(\sigma_{sol}\nabla\phi_{sol}) + S_{\phi,sol} = 0$	CB; CB	CB; CB	SF=0 - SF=0	SF=0 - SF=0	SF=0 - SF=0
		CB; SV=0	PJ - SF=0	PJ - ND	ND - PJ	PJ - PJ
		CB; CB	SF=0 - SF=0	SF=0 - SF=0	SF=0 - SF=0	SF=0 - SF=0
Membrane potential	$\nabla.(\sigma_{mem}\nabla\phi_{mem}) + S_{\phi,mem} = 0$	CB; CB	CB; CB	SF=0 - SF=0	SF=0 - SF=0	SF=0 - SF=0
		CB; SF=0	PJ - SF=0	PJ - ND	ND - PJ	PJ - PJ
		CB; CB	SF=0 - SF=0	SF=0 - SF=0	SF=0 - SF=0	SF=0 - SF=0
Energy	$\nabla(\rho\varepsilon\vec{u}h) = \nabla(k^{eff}\nabla T) + S_h$	HF=0; HF=0	CB; CB	HF=0 - HF=0	HF=0 - HF=0	HF=0 - HF=0
		CB; T=353 K	PJ - HF=0	PJ - ND	ND - PJ	PJ - PJ
		HF=0; HF=0	T=353 K - T=300	HF=0 - HF=0	HF=0 - HF=0	HF=0 - HF=0

Table 8.Conservation equations and boundary conditions of cathode side of PEMFC.

	Conservation Equations	Boundary Conditions of Cathode Side Throgh x, y and z Axis				
		CCC	CGC	CGDL	CCL	Membrane
Mass	$\nabla(\rho\varepsilon\vec{u}) = S_m$	ZDF – ZDF	ZDF – ZDF	ZDF – ZDF	ZDF – ZDF	ZDF – ZDF
		ZDF – ZDF	PJ – ZDF	PJ – ND	ND – PJ	PJ – PJ
		ZDF – ZDF	MFI – SV=0	ZDF – ZDF	ZDF – ZDF	ZDF – ZDF
Momentum	$\nabla(\rho\varepsilon\vec{u}\vec{u}) = -\varepsilon\nabla p + \nabla\cdot\varepsilon\mu\nabla\vec{u} + S_u$	NS – NS	NS – NS	NS – NS	NS – NS	NS – NS
		NS – NS	PJ – NS	PJ – ND	ND – PJ	PJ – PJ
		NS – NS	MFI – PO (P=0)	NS – NS	NS – NS	NS – NS
Species	$\nabla(\varepsilon\vec{u}C_k) = \nabla(D_k^{eff}\nabla C_k) + S_k$	ZDF – ZDF	ZDF – ZDF	ZDF – ZDF	ZDF – ZDF	ZDF – ZDF
		ZDF – ZDF	PJ – ZDF	PJ – ND	ND – PJ	PJ – PJ
		ZDF – ZDF	MFI – SV=0	ZDF – ZDF	ZDF – ZDF	ZDF – ZDF
Solid Phase Potential	$\nabla.(\sigma_{sol}\nabla\phi_{sol}) + S_{\phi,sol} = 0$	CB; CB	CB; CB	SF=0 – SF=0	SF=0 – SF=0	SF=0 – SF=0
		SV=V_{cell} ; CB	PJ – SF=0	PJ – ND	ND – PJ	PJ – PJ
		CB; CB	SF=0 – SF=0	SF=0 – SF=0	SF=0 – SF=0	SF=0 – SF=0
Membrane Potential	$\nabla.(\sigma_{mem}\nabla\phi_{mem}) + S_{\phi,mem} = 0$	CB; CB	CB; CB	SF=0 – SF=0	SF=0 – SF=0	SF=0 – SF=0
		SF=0; CB	PJ – SF=0	PJ – ND	ND – PJ	PJ – PJ
		CB; CB	SF=0 – SF=0	SF=0 – SF=0	SF=0 – SF=0	SF=0 – SF=0
Energy	$\nabla(\rho\varepsilon\vec{u}h) = \nabla(k^{eff}\nabla T) + S_h$	HF=0; HF=0	CB; CB	HF=0 – HF=0	HF=0 – HF=0	HF=0 – HF=0
		T=353 K; CB	PJ – HF=0	PJ – ND	ND – PJ	PJ – PJ
		HF=0; HF=0	T=353 K – T=300	HF=0 – HF=0	HF=0 – HF=0	HF=0 – HF=0

Table 9.Number of grid distributions for PEMFC layers with hexagonal structure at five different grid spacings.

PEMFC Layers (Grid spacing)	Number of Grids (0.25	0.40	0.50	0.60	1.00)	Aspect ratio
Current Collector	129920	35700	16240	9126	2030	35
Gas Channel	4480	1575	560	468	70	70
Gas Diffusion Layer	21280	9975	5320	4446	1330	233
Catalyst Layer	21280	9975	5320	4446	1330	5426
Membrane	21280	9975	5320	4446	1330	648
Cell	446880	149625	69160	48906	11970	14,7

4.1. Tests for the Grid Independent Solutions

The minimum number of mesh in the solution domain was restricted due to the high aspect ratio. The distribution of mesh numbers for each layer and grid structures is presented in Table 9. The solutions were obtained for the five different grid structures as shown in Table 10 in order to test the results to be independent from the number of meshes used. The decision criterion for the determination of the grid independent solutions was that the deviation in the current density be less than unity. However, the solution time was also an important parameter to decide the sufficient number of meshes. It was concluded that the mesh number of 69160 was the most suitable structure after analyzing the solutions.

Table 10. Mean current density values [a] and solution times at different number of grids.

Interval Size	Total no. of grids	Current Density / A cm^{-2}	Dev. in Current Density / %	Solution Time / min
1.00	11970	81,13918	-	10
0.60	48906	82,34035	1,4	33
0.50	69160	83,06287	0,88	41
0.40	149625	83,25338	0,23	88
0.25	446880	83,61678	0,44	1139

[a] solutions were obtained by using the parameters for Case 1

4.2. Polarization Curves

The total cell over potential was defined as the difference between the theoretical open cell voltage and cell voltage. The theoretical open cell voltage was calculated as 1.18 V for the cell analyzed [15]. Therefore, each cell over potential was corresponded to a cell voltage. The current density values were computed from the numerical model corresponding to the over-potential values (the cell voltage). The total cell over-potential was increased by a step function like a hyperbolic relaxation function [16]. The seven over potential steps were determined as 0.23, 0.28, 0.33, 0.38, 0.58, 0.78, and 0.88 V. The polarization curve was constructed using the computed current density values and cell voltage values for these seven steps [15]. The results reached from a converged solution were taken as the initial values for the solved quantities at the next solution step.

The open circuit voltage values were calculated using the theoretical open circuit voltage value and taking into account the voltage loss due to the activation energy. The following equation was used to calculate the true open circuit voltage value [17],

$$V = E - A\ln\left(\frac{I + I_n}{I_o}\right) \tag{10}$$

where I_o and I_n were represented an exchange current density and internal current density, respectively. The symbol, E was called the theoretical open circuit voltage when no current passed through the circuit. The value of the theoretical open circuit voltage was calculated as 1.18 V for the fuel cell [15]. The open circuit voltage was calculated as 0.92 V using Eq.(7.10) and taking the fuel cell parameters such as the reference current density (I_o = 0,04 mA cm^{-2}), crossover current (I_n=3 mA cm^{-2}) and coefficient in the Tafel equation (A=0.06 V) for the fuel cell studied.

4.3. The Convergence Criteria

It was assumed that the convergence was obtained when the residual value for each solved property except energy reached to 10^{-4} and the residual value for the energy reached to 10^{-6}.

Table 11.Operational parameters [c] for Fluent PEMFC Module.

Case No	Pressure / Atm.	Mass Flux / kg s^{-1}		Mass Fraction			
		(Anode)	(Cathode)	(Anode)		(Cathode)	
				H_2	H_2O	O_2	H_2O
1	1,5	10^{-7}	10^{-6}	0,95	0,05	0,23	0,01
2	2	10^{-7}	10^{-6}	0,95	0,05	0,23	0,01
3	3	10^{-7}	10^{-6}	0,95	0,05	0,23	0,01
4	1,5	10^{-6}	10^{-6}	0,95	0,05	0,23	0,01
5	1,5	10^{-5}	10^{-6}	0,95	0,05	0,23	0,01
6	1,5	10^{-7}	10^{-4}	0,95	0,05	0,23	0,01
7	1,5	10^{-7}	10^{-5}	0,95	0,05	0,23	0,01
8	1,5	10^{-7}	10^{-6}	0,90	0,10	0,23	0,01
9	1,5	10^{-7}	10^{-6}	0,60	0,40	0,23	0,01
10	1,5	10^{-7}	10^{-6}	0,38	0,62	0,23	0,01
11	1,5	10^{-7}	10^{-6}	0,95	0,05	0,21	0,10
12	1,5	10^{-7}	10^{-6}	0,95	0,05	0,25	0,20

[c] Operational pressure is atmospheric pressure for all 9 cases.

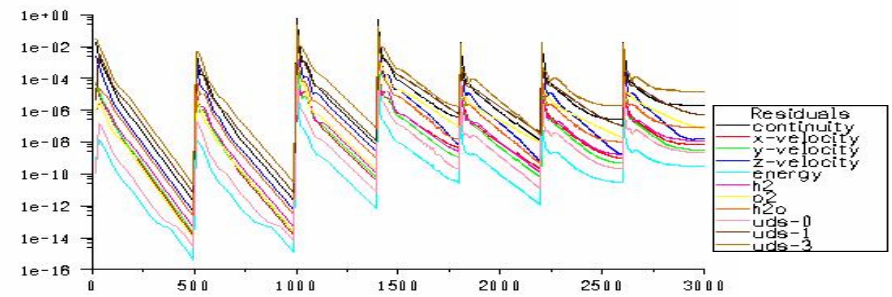

Figure 2. Convergence plot for case 2: Variation of residuals for solved quantities with iteration number.

The computer model of the problem was run for the twelve cases which their operational parameters presented in Table 11. The convergence plot for the Case 2 is presented in Fig. 2. The variation of residuals for the solved quantities – the continuity, momentum, energy, chemical species (H_2, O_2, H_2O), solid phase potential (UDS-0), membrane phase potential (UDS-1) and water content (UDS-3) - were plotted against the iteration number. In Fig.2, it is shown that all the residuals are under the value of 10^{-10} at the five hundredth iterations. The program was interrupted at the 500^{th} iteration and the obtained cell potential was given as an initial condition to the cell for the next iteration. The polarization curves for the twelve different cases were constructed by renewing the seven successive cell potential values and reaching up to 3000 iterations with the residuals under the value of 10^{-4}. The reason for renewing the values of the cell potential at the boundaries was to reduce the solution time to an appropriate level.

According to Fig. 2, all the residual values for the first two successive solutions are under the value of 10^{-10} and the residual values between the third and the seventh solutions are under the value of 10^{-4}. It was noted that the residual value for the energy equation must be under the value of 10^{-6}. The convergence was obtained at the 500^{th} iteration for the first two solutions and at the 400^{th} iteration for the five successive solutions after the first two one. It can be concluded that the converged solution is obtained at the end of the seven successive solutions for the corresponding over-potential values. This procedure was applied to the twelve different cases to construct the polarization curves.

5. COMPARISON WITH THE EXPERIMENT

An experimental study belongs to Wang et. al. [10] was used to verify the numerical results. The experiments were performed at the atmospheric pressure and cell temperature of 70°C. The volumetric flow rate of the

anode and cathode gases were given at the standard state conditions as 1200 and 2100 S-cm^3 min^{-1} in the experiments, respectively. These data were converted to the required inputs in FLUENT as given in Table 12. The methodology of conversion process is explained in the thesis of Alpat [15]. The variation of current density values with the voltage is presented in Fig. 3 for both the numerical and experimental cases. The open circuit voltage was 0.88 V for the test case. As shown in Fig. 3, close current density values were obtained at the voltages higher than 0.68 V. Although there is some discrepancy at the specific voltage values, the same trend is obtained for the current density variation as a whole. The limitation in the current density at low voltages is clearly seen as tracking the experimental data. The deviation between the numerical and experimental data at the limiting values of current density is possibly due to the lack of liquid phase in the model.

Table 12. FLUENT inputs corresponding to operational data in the experiment [10]

$\dot{m}_{an}$ / kg s^{-1} / 10^{-5}	$\dot{m}_{cat}$ / kg s^{-1} / 10^{-5}	Mass fractions of anode gases		Mass fractions of cathode gases		
		y_{H_2}	y_{H_2O}	y_{O_2}	y_{H_2O}	y_{N_2}
0,5398	3,2940	0,2010	0,7989	0,2125	0,0826	0,7004

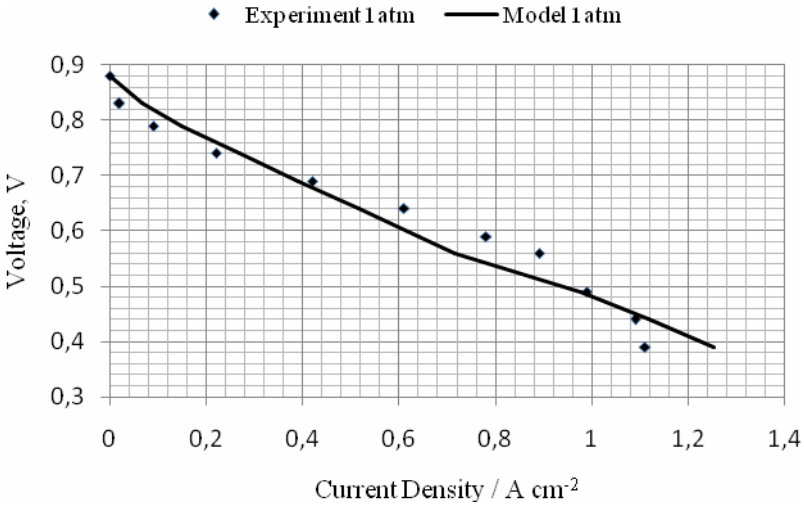

Figure 3. Comparison of numerical predictions with the experiment.

While the model was predict the magnitude of the current produced fairly well, the characteristic features of the activation, ohmic, and concentration regions could not be reflected well. This defect of the model should be kept in mind when analyzing the behavior of the cell to the changes in operating parameters.

6.RESULTS

Solutions were obtained for the twelve different cases as shown in Table 11 using the structure with mesh number of 69160 on the PEMFC model which was constructed and analyzed using the FLUENT PEMFC module. Solver data was obtained using a PC of 1.73 GHz Pentium 4 and is presented in Table 13.

The converged solution was obtained at the 500th iteration for the first step for each case except the fifth and sixth cases. It was seen that the iteration number gradually decreased for the successive solution steps. The total solution time was less than the 3500 iterations for all the other cases except the Case 6. It was observed that the mass flow rate of the cathode had a dominant effect on the solution time.

Table 13. Solver data.

Solver Data	Values
Total mesh number	69160
RAM-used/RAM-available	590/760MB
Total iteration number	500
Mean time per one iteration	4 seconds
Total iteration time	2495 seconds (42 min.)
Required time for 7 point polarization curve	237 minute (4 hour)

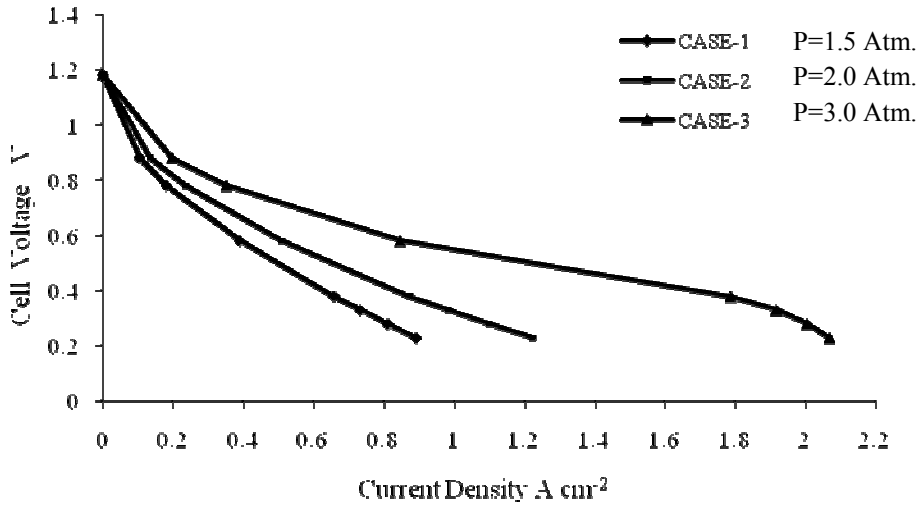

Figure 4. The effect of pressure on polarization curves.

The results were presented as polarization curves showing the effect of five different parameters; the pressure, mass flow rate of the anode side, mass flow rate of the cathode side, mass fraction of the hydrogen and mass fraction of the water at the cathode side. The polarization curves were compared with three different values of each parameter. The effect of pressure on polarization curve is shown in Fig. 4. The hydrogen fuel was sent to the fuel cell at three different pressures; 1.5 Atm. (Case 1), 2.0 Atm. (Case 2) and 3.0 Atm. (Case 3). The current density value was reached to 0.89 A cm^{-2} when the cell voltage value dropped to 0.23V at the operation pressure of 1.5 Atm. The current density value was increased from 0.89 A cm^{-2} to 1.22 A cm^{-2}, 37%, and 2.07 A cm^{-2}, 70%, at 0.23V when the pressure increased from 1.5 Atm. to 2.0 and 3.0 Atm., respectively. The difference between the current density values was increased for three different cell pressures when the cell voltage dropped to 0.23 V.

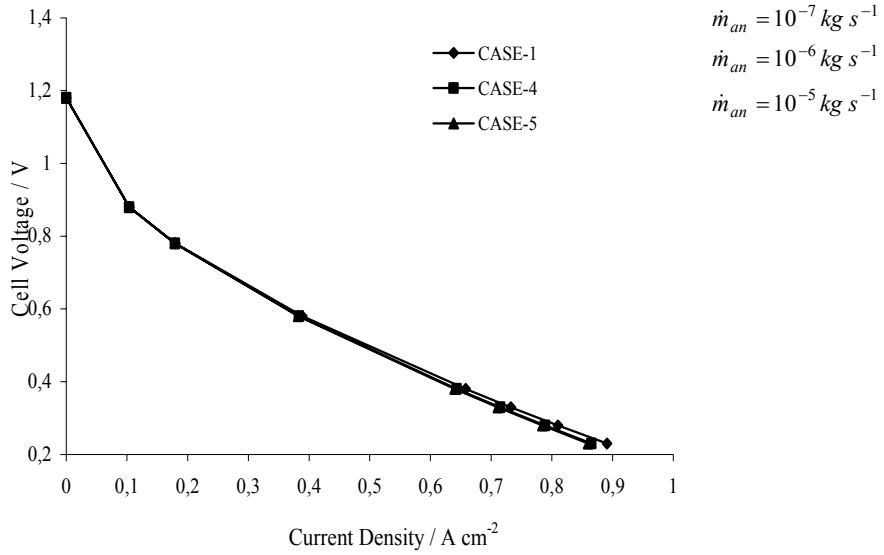

Figure 5. The effect of mass flow rate of anode gases on polarization curves.

The effect of mass flow rate of the anode gases on polarization curves is shown in Fig. 5. The three cases (Case1, 4 and 5) are compared in Figure 5. The mass flow rate of the anode gases was increased from the value of 10^{-7} kg s^{-1} (Case 1) to 10^{-6} (Case 4) and 10^{-5} (Case 5) kg s^{-1}, respectively. It was shown that there was no considerable change in the current density value while increasing the cell voltage for these three mass flow rates of the anode gases.

The effect of the mass flow rate of cathode gases on the polarization curves is shown in Fig. 6. The mass flow rate of the cathode gases was increased from the value of 10^{-6} kg s^{-1} (case 1) to 10^{-5} kg s^{-1} (case 7) and 10^{-4} kg s^{-1} (case 6), respectively. It was shown that the current density decreases dramatically from the value of 0.89 A cm^{-2} to 0.45 A cm^{-2}, 50%, and 0.36, 8%, corresponding to the cell voltage value of 0.23 V when increasing the mass flow rate of the cathode gases from the value of 10^{-6} kg s^{-1} to 10^{-5} kg s^{-1} and 10^{-4} kg s^{-1}, respectively. It was also shown that the effect of pressure on the current density increased as the cell voltage had been dropped.

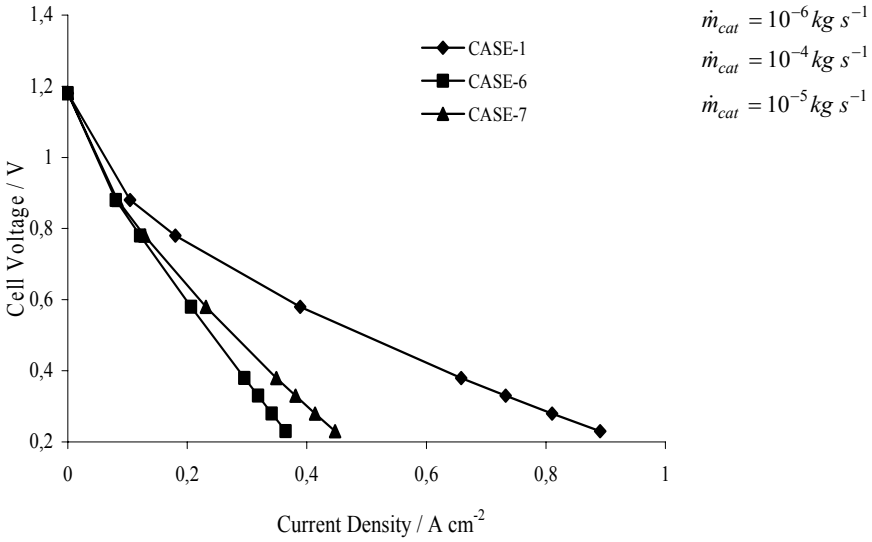

Figure 6. The effect of mass flow rate of cathode gases on polarization curves.

The effect of the mass fraction of hydrogen on the polarization curves is shown in Fig. 7. The mass fraction of the hydrogen was decreased from the value of 0.95 (Case 1) to 0.60 (Case 9) and 0.38 (Case 10), respectively. It was surprisingly shown that the current density increased from the value of 0.89 A cm^{-2} to 1.48 A cm^{-2}, 63%, and 1.83 A cm^{-2}, 24%, corresponding to the cell voltage value of 0.23 V when decreasing the mass fraction of hydrogen from the value of 0.95 to 0.60 and 0.38, respectively. It was also shown that the effect of mass fraction of hydrogen on the current density gradually increased as the cell voltage dropped.

The effect of mass fraction of water at the cathode side on the polarization curve is shown in Fig. 8. The mass fraction of water was increased from the value of 0.01 (Case 1), to 0.10 (Case 11) and 0.20 (Case 12), respectively. It was shown that the current density increased from the value of 0.89 A cm^{-2} to 1.77 A cm^{-2}, 99%, and 2.43 A cm^{-2}, 37%, corresponding to the cell voltage value of 0.23 V when increasing the mass fraction of water from the value of 0.01 to 0.10 and 0.20, respectively. It was also shown that the effect of mass fraction of water at the cathode side on the current density gradually increased as the cell voltage had been dropped.

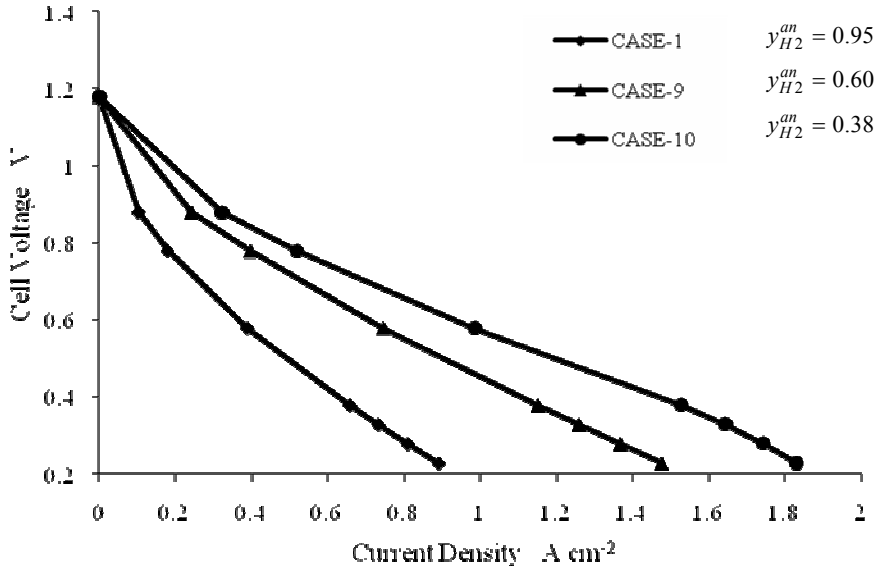

Figure7. The effect of mass fraction of hydrogen on polarization curves.

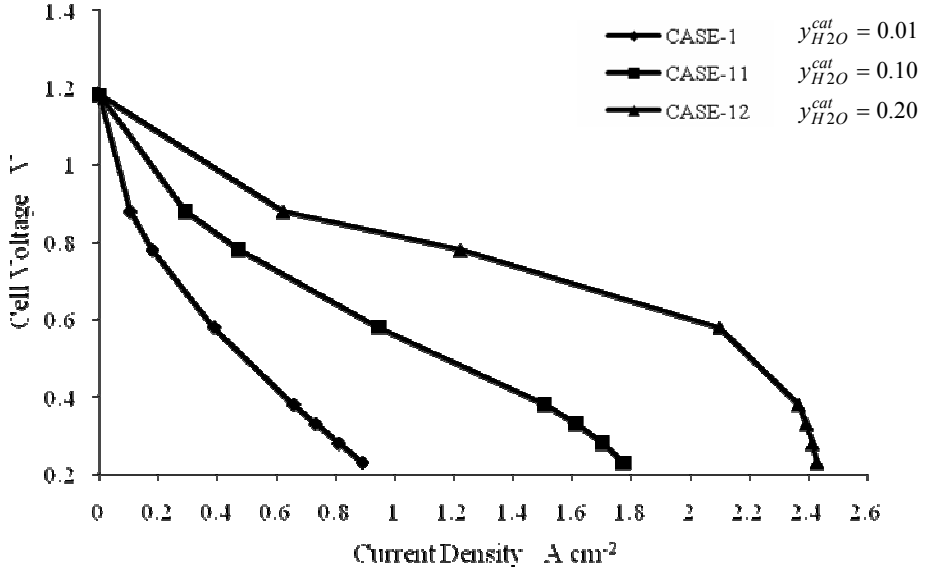

Figure 8. The effect of mass fraction of water at the cathode side on polarization curves.

CONCLUSION

The polarization curves were showed that the mass flow rate of anode gases had weak effects on the current density rather than that of the cathode'. Besides, the mass fraction of water on the cathode side was more dominant than the one on the anode side over the production of current. Consequently, adjusting the mass flow rate and mass fractions of gases on the cathode side was much more effective than the anode side gases to reach high current densities. The higher current density was obtained at the lower mass fraction of hydrogen and the higher mass fraction of water at the cathode side. Therefore, there must be an optimum point which maximizes the current density. One can obtain this optimum by regulating the mass fractions of cathode side and also the mass flux of cathode gas. It was more appropriate to balance the mass fractions rather than the mass flux of cathode gasses. As a result, the suggestion was that it was more advantageous to adjust the mass flow rate of cathode gases and the mass fraction of water on the both sides. The current density was more dependent on the mass fraction of water on the cathode side rather than the mass fraction of hydrogen. Therefore, a controlling parameter should be selected as the mass fraction of water on the cathode side. Although it was easy to control the current density via balancing the mass fraction of water on the cathode side, the limitation on current density was occurred at lower voltage values. Increasing the mass fraction of water on the cathode side was increased the limitation on the current density due to the blockage effect of the water after a limiting value. Furthermore, operating at high pressures also was increased the current production but operational problems should have not been ignored due to the gas leakage, etc. Moreover, the mass transfer limitation was seen more clearly at higher pressures than the atmospheric one as shown in Fig. 4. Comparing the cases in this figure, the slope of polarization curve at lower voltages was seen increased at higher pressures. This is a clear evidence of mass transfer limitation although the value of current density was increased.

ACKNOWLEDGEMENT

The authors gratefully acknowledge the Mechanical Engineering Department of Gazi University for its financial support and for permission to use the FLUENT software. The authors would also like to thank the Clean Energy Research Center of Gazi University for the Permission to use the PEM fuel cell module of FLUENT 6.2.

REFERENCES

[1] Berning, T., Lu, D.M., Djilali, N., "Three-dimensional computational analysis of transport phenomena in a PEMFC", ***J Power Sources***, 106(1-2): 284-294 (2002).

[2] Mazumder, S., Cole, J.V., "Rigorous 3-D mathematical modeling of PEM fuel cells II. Model predictions with liquid water transport", ***J Electrochem. Soc.***, 150(11):A1510-1517 (2003).

[3] Ju, H., Meng, H., Wang, C.Y., "A single-phase, non-isothermal model for PEM fuel cells", ***Int J Heat Mass Transfer***, 48(7):1303-1315 (2005).

[4] Wang, Y., Wang, C.Y., "Electron Transport in PEFCs", ***J Electrochem. Soc.***, 151(3):A358-A367 (2004).

[5] Wang, Y., Wang, C.Y., "A Non-isothermal, Two-Phase Model for Polymer Electrolyte Fuel Cells", ***Electrochem.***, 153(6):A1193-A1200 (2006).

[6] Pasaogulları, U., Wang, C.Y., "Liquid water transport in gas diffuser layer of polymer electrolyte fuel cells", ***J. Electrochem. Soc.***, 151(3):A399-A406 (2004).

[7] Ju, H., Wang, C.Y., "Experimental validation of a PEM fuel cell model by current distribution data", ***J. Electrochem. Soc.***, 151(11):A1954-A1960 (2004).

[8] Meng, H., Wang, C.Y., "Large-scale simulation of polymer electrolyte fuel cells by parallel computing", ***Chem. Eng. Sci.***, 59(16):3331-3343 (2004).

[9] Um, S., Wang, C.Y., Chen, K.S., "Computational Fluid Dynamics Modeling of Proton Exchange Membrane Fuel Cells", ***J. Electrochem. Soc.***, 147(12): 4485-4493 (2000).

[10] Wang, L., Husar, A., Zhou, T., Liu, H., "A parametric study of PEM fuel cell performances", ***Int. J. Hydrogen Energy***, 28:1263-1272 (2003).

[11] Kumar, A., Reddy, R.G., "Modeling of Polymer Electrolyte membrane fuel cell with metal foam in the flow-field of the bipolar/end plates", ***J. Power Sources***, 114:54-62 (2003).

[12] Jiao, K., Zhou, B., Quan, P., "Liquid water transport in parallel serpentine channels with manifolds on cathode side of a PEM fuel cell stack", ***J. Power Sources***, 154:124–137 (2006).

[13] Quan, P., Lai, M.C., "Numerical study of water management in the air flow channel of a PEM fuel cell cathode", ***J. Power Sources***, 164:222–237 (2007).

[14] Jiao, K., Zhou, B., "Innovative gas diffusion layers and their water removal characteristics in PEM fuel cell cathode", ***J. Power Sources***, 169:296–314 (2007).

[15] Alpat, C.Ö., "Numerical Solution of a Proton Exchange Membrane Fuel Cell with Straight Channels", MSc. Thesis, ***Institute of Science and Technology***, Gazi University, Ankara, 201 (2007).

[16] Siegel, N.P., "Development and Validation of a Computational Model for a Proton Exchange Membrane Fuel Cell", PhD Thesis, the Faculty of Virginia Polytechnic Institute and State University, Virginia, (2003).

[17] Larminie, J., Dicks, A., "Fuel Cell Systems Explained", ***U.K.: John Wiley***, 2nd Ed. (2003).

NOMENCLATURE

A	Constant in Eq. (10), $RT/2\alpha F$
C	Concentration, mol/cm^3
D	Diffusivity, m^2/s
E	Open circuit voltage, V
F	Faraday's constant, 96487 C/equivalent
h	Enthalpy, kJ/kg
I	Current density, A/cm^2
I_o	Exchange current density, A/cm^2
I_n	Internal current density, A/cm^2
n	Constant in Eq. (3b)
p	Pressure
R	Volumetric transfer current, A/m^3
S	Source Term, W/m^3
t	Time, s
T	Temperature, ^{o}C
u	Velocity in x-direction, m/s
V	Voltage, V
x	Coordinate axis in x-direction

Greek Symbols

ε	Porosity of the porous media
μ	Viscosity, kg/m s
ρ	Density, kg/m^3
η	Over-potential, V
σ	Ionic conductivity, S/m
Φ	Electrical potential, V
ϕ	Dependent variable
Γ	Effective diffusion coefficient, m^2/s

Subscripts

k	species index, 1 to n
react	reaction
an	anode
cat	cathode
ohm	ohmic
L	latent
u	velocity in x direction
e	electrolyte
mem	membrane
Sol	solid
avg	average
h	enthalpy
i	dummy index in Eq. (9)
j	index in Eq. (3b)
o	reference state

Superscripts

eff	effective

Abbreviations

CFD	Computational Fluid Dynamics
CB	Collective Boundary
FC	Fuel Cell
GDL	Gas Diffusion Layer
HF	Heat Flux
MEA	Membrane Electrode Assembly
MFI	Mass Flow Inlet
ND	Not Defined
NS	No Slip
PEM	Proton Exchange Membrane
PO	Pressure Outlet (=P_o)
PJ	Porous Jump
SV	Specified Value
SF	Specified Flux
UDS	User Defined Scalar
ZDF	Zero Diffusive Flux